

RESEARCH ARTICLE

*Electronic Cigarettes: Not All Good News?*

## Menthol in electronic cigarettes causes biophysical inhibition of pulmonary surfactant

Lu Xu,<sup>1</sup> Yi Yang,<sup>1</sup> Jennifer Michelle Simien,<sup>2</sup> Christopher Kang,<sup>2</sup> Guangle Li,<sup>1</sup> Xiaojie Xu,<sup>1</sup> Ellinor Haglund,<sup>2</sup> Rui Sun,<sup>2</sup> and Yi Y. Zuo<sup>1,3</sup>

<sup>1</sup>Department of Mechanical Engineering, University of Hawaii at Manoa, Honolulu, Hawaii; <sup>2</sup>Department of Chemistry, University of Hawaii at Manoa, Honolulu, Hawaii; and <sup>3</sup>Department of Pediatrics, John A. Burns School of Medicine, University of Hawaii, Honolulu, Hawaii

### Abstract

With an increasing prevalence of electronic cigarette (e-cigarette) use, especially among youth, there is an urgent need to better understand the biological risks and pathophysiology of health conditions related to e-cigarettes. A majority of e-cigarette aerosols are in the submicron size and would deposit in the alveolar region of the lung, where they must first interact with the endogenous pulmonary surfactant. To date, little is known whether e-cigarette aerosols have an adverse impact on the pulmonary surfactant. We have systematically studied the effect of individual e-cigarette ingredients on an animal-derived clinical surfactant preparation, bovine lipid extract surfactant, using a combination of biophysical and analytical techniques, including in vitro biophysical simulations using constrained drop surfactometry, molecular imaging with atomic force microscopy, chemical assays using carbon nuclear magnetic resonance and circular dichroism, and in silico molecular dynamics simulations. All data collectively suggest that flavorings used in e-cigarettes, especially menthol, play a predominant role in inhibiting the biophysical function of the surfactant. The mechanism of biophysical inhibition appears to involve menthol interactions with both phospholipids and hydrophobic proteins of the natural surfactant. These results provide novel insights into the understanding of the health impact of e-cigarettes and may contribute to better regulation of e-cigarette products.

*constrained drop surfactometry; electronic cigarette; flavor; menthol; pulmonary surfactant*

### INTRODUCTION

Electronic cigarettes (e-cigarettes) are battery-powered nicotine-delivery devices that produce inhalable aerosols without actual combustion (1). E-cigarettes use various flavorings to mask the harsh taste of nicotine and aldehydes produced during vaping (2). Flavorings are used in e-cigarettes as a major marketing tool to attract youth, young adult, and adult users (3). The number of youths in the United States who have ever used an e-cigarette tripled every year between 2011 and 2014 (4). The Centers for Disease Control and Prevention (CDC) have ranked e-cigarettes as the most commonly used nicotine-delivery device among US youth, with minors more likely than adults to use the device. The global market of e-cigarettes was estimated to be worth \$8 billion in 2015, and it is expected to expand to more than \$80 billion by 2025 (5).

E-cigarettes were initially advertised as a healthier and safer alternative to conventional tobacco smoking, when they first appeared in the mid-2000s. However, increasing

research evidence, especially long-term (>10 yr) toxicological data that emerged only in recent years, has suggested that e-cigarettes are not as safe as originally promised. It was found that e-cigarette aerosols contain a variety of toxic chemical components (6–8). The use of e-cigarettes has become an established risk factor for a range of pulmonary (9, 10) and cardiovascular (11) diseases (12). The use of e-cigarettes has been linked to asthma and other chronic lung diseases in adolescents (13). It was found that chronic exposure to e-cigarette aerosols can alter lipid homeostasis in the lung (14), downregulate innate immunity, damage DNA and thus increase the risk of lung cancer (15), and cause adverse neurodevelopmental outcomes in a prenatal mouse model (16). The CDC has reported more than 2,000 fatal cases of electronic cigarette, or vaping, product use-associated lung injury (EVALI) (17, 18). Hence, there is an urgent need to better understand the biological risks of e-cigarettes and the pathophysiology of health conditions related to the use of e-cigarettes.

It is estimated that each puff produces an average of  $6.25 \times 10^{10}$  inhalable e-cigarette aerosols (ECAs) (19). A

majority of these aerosols are in the submicron size, ranging from 100 to 500 nm (20–23), which end up depositing in the alveolar region of the lung (19, 24). Once reaching alveoli, the aerosols must first interact with the pulmonary surfactant (PS) that lines the entire alveolar surface as a thin film (25). The PS consists of ~80 wt% phospholipids, 5%–10% neutral lipids (mainly cholesterol), and 5%–10% proteins (26). Its major biophysical and physiological function is to reduce the alveolar surface tension to near-zero values, thereby maintaining a large surface area of the lung for effective gas exchange during normal tidal breathing. Dysfunction of PS leads to life-threatening respiratory diseases such as acute respiratory distress syndrome (ARDS) (27, 28). It was estimated that after only 10 puffs, the thickness of ECAs deposited in the lung would be comparable to that of the PS film (19). In spite of extensive reports of *in vitro*, *in vivo*, and clinical studies performed to better understand the toxicological effect and health risk of ECAs (12), little is known about how inhaled ECAs interact with the PS film, and whether ECAs have an adverse impact on the biophysical function of the PS film.

Here we studied the biophysical impact of ECAs on a natural, animal-derived PS, *i.e.*, bovine lipid extract surfactant (BLES), using a newly developed experimental methodology called constrained drop surfactometry (CDS). CDS is a new generation of droplet-based surface tensiometry technique that allows for high-fidelity biophysical simulation of nanoparticle interactions with natural PS under physiologically relevant conditions (29, 30). With biophysical assessments using CDS, molecular visualization using atomic force microscopy (AFM), chemical assays using carbon nuclear magnetic resonance (<sup>13</sup>C-NMR) and circular dichroism (CD), and *in silico* molecular dynamics (MD) simulations, we have systematically studied the biophysical impact of individual e-cigarette liquid (e-liquid) components on the PS film. All data collectively suggest that flavorings used in e-cigarettes, especially menthol, rather than nicotine, play a predominant role in inhibiting the biophysical function of natural PS. The mechanism of biophysical inhibition appears to involve menthol interactions with both phospholipids and proteins in the PS. These results provide novel insights into the understanding of health impact of e-cigarettes and may contribute to a better regulation of e-cigarette products.

## MATERIALS AND METHODS

### Materials

Bovine lipid extract surfactant (BLES) was obtained from BLES Biochemicals (London, ON, Canada). BLES is a modified natural PS prepared from bronchopulmonary lavage of adult cows with organic solvent extraction. It contains all hydrophobic components of the bovine natural surfactant, including the hydrophobic surfactant proteins, SP-B and SP-C, with a reduced cholesterol content (26). The hydrophilic surfactant proteins, SP-A and SP-D, were removed during the extraction process. BLES was stored in sterilized vials at an initial phospholipid concentration of 27 mg/mL. It was diluted to 0.5 mg/mL using a saline buffer (0.9% NaCl, 1.5 mM CaCl<sub>2</sub> and 2.5 mM HEPES at pH 7.0) on the day of experiments. Alternatively, for the study of spread films,

BLES was extracted using a chloroform-methanol mixture, dried under a nitrogen stream, and resuspended in chloroform to a final concentration of 1 mg/mL.

A commercial menthol-flavored e-liquid (Black Note, Irvine, CA) that contains 6 mg/mL nicotine in a 50/50 (vol/vol) mixture of propylene glycol (PG) and vegetable glycerin (VG) was studied as a representative e-liquid. To study the effect of individual chemical ingredients of the e-liquid, we have prepared recombinant e-liquids using the 50/50 mixture of PG (CAS 57-55-6) and VG (CAS 56-81-5) as the vehicle solvent. Major chemical ingredients of the recombinant e-liquids are nicotine (6 mg/mL, CAS 22083-74-5) and menthol (12 mg/mL, CAS 89-78-1), matching the chemical composition and concentration used in the commercial e-liquid. For comparison, we have studied two more popular flavor chemicals, *i.e.*, ethyl maltol (10 mg/mL, CAS 4940-11-8) and ethyl butyrate (7.4 mg/mL, CAS 105-54-4), at the median concentration used in e-cigarette products (2, 31). All chemicals were purchased from Sigma-Aldrich and used without further purification.

### Constrained Drop Surfactometry

Constrained drop surfactometry (CDS) is a new generation of droplet-based tensiometry technique developed in our laboratory for biophysical study of PS and its interactions with nanoparticles (29, 30). As shown in Fig. 1, it uses the air-water surface of a 4-mm sessile droplet to accommodate the adsorbed or spread PS film. The droplet is “constrained” on a pedestal that uses a knife-sharp edge to prevent film leakage at low surface tensions. The PS film can be compressed and expanded quasi-statically or dynamically by controlling liquid flow out of and into the droplet using a motorized syringe. The surface tension and surface area of the PS film are determined simultaneously from the shape of the droplet using closed-loop axisymmetric drop shape analysis (CL-ADSA) (32). The droplet is enclosed in an environmental chamber capable of controlling physiologically relevant conditions, *i.e.*, the core body temperature at 37°C and a relative humidity (RH) close to 100%, or a polluted environment by airborne particles (29).

E-cigarette aerosols (ECAs) were generated using a homemade negative-pressure ECA generator (33, 34). As illustrated in Fig. 1, the ECA generator consists of a third-generation modifiable e-cigarette device (Geekvape Aegis Mini) and a motorized syringe that allows a precise control of the puffing profile. This modifiable device (“mod”) contains a refillable sub-ohm tank with a M1+ mesh coil of resistance 0.16 Ω. The power of this e-cigarette device can be adjusted between 5 and 80 W, corresponding to a temperature range between 100°C and 315°C. The e-cigarette device was operated at 60 W for consistency. The puff duration and the time break between two puffs were controlled at 3 and 25 s, to simulate vaping (35–37). The aerosols were subsequently delivered into the CDS chamber and were exposed to the BLES film in a dose-controlled manner to mimic ECA inhalation.

After exposure to the aerosols, the BLES film was periodically compressed and expanded at 20 cycles per min with a compression ratio of no more than 20% of the initial surface area, at 37°C and 100% RH to simulate normal tidal

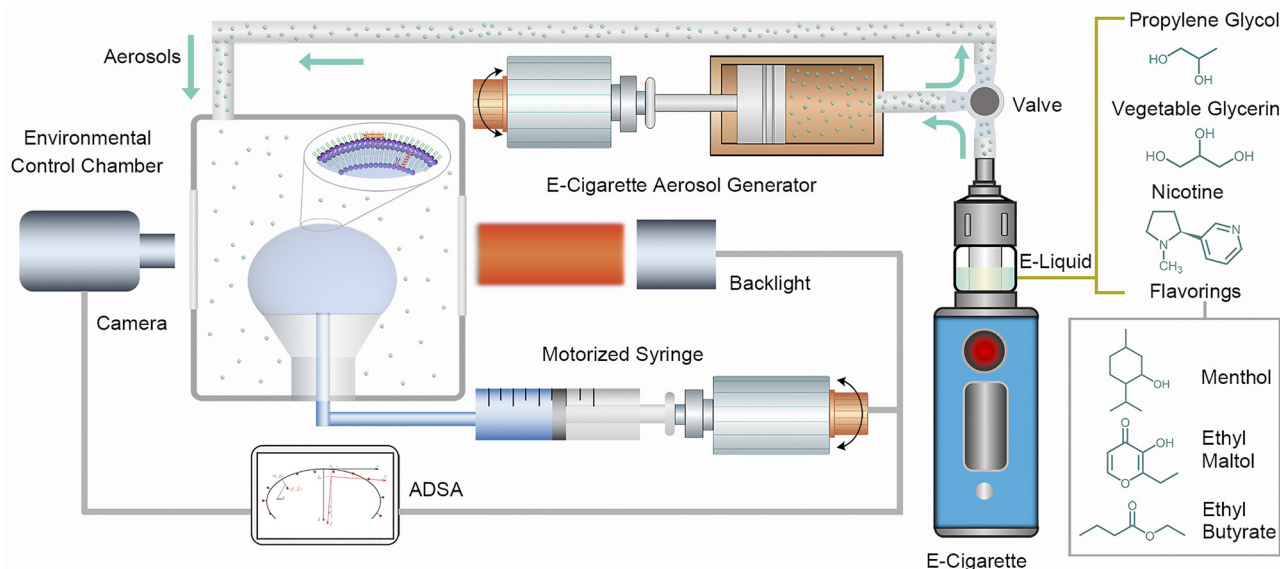


**Figure 1.** Schematic of constrained drop surfactometry (CDS) in combination with an electronic cigarette aerosol (ECA) generator. The ECA generator consists of a commercial e-cigarette device with a refillable cartridge, and a negative-pressure puff simulator powered by a motorized syringe. ECAs generated by simulated puffs are collected in the syringe and are delivered to the environmental chamber of the CDS, in which the PS film is exposed to ECAs with controlled dosimetry. CDS uses the air-water surface of a 4-mm sessile droplet to accommodate an adsorbed or spread PS film. The droplet is constrained on a pedestal with a sharp knife-edge and is enclosed in an environmental chamber capable of simulating physiologically relevant conditions. The surfactant film can be periodically compressed and expanded by precisely controlling liquid flow out of and into the droplet using a motorized syringe. The surface tension and surface area of the PS film are simultaneously determined from the shape of the droplet using closed-loop axisymmetric drop shape analysis (CL-ADSA). PS, pulmonary surfactant.

breathing (38). Biophysical properties of the BLES film, with and without exposure to the aerosols, were assessed with the minimum surface tension ( $\gamma_{\min}$ ) at the end of compression and the isothermal film compressibility ( $\kappa_{\text{comp}}$ ) (29, 30). To determine the quasi-static surface activity of the PS film, monolayers of BLES or BLES/menthol mixtures were spread to the air-water surface of a droplet, at room temperature. The droplet was slowly expanded to increase the surface tension until the corresponding surface pressure was lowered to around 1 mN/m. The droplet was left undisturbed for  $\sim 1$  min to allow chloroform evaporation. The spread BLES or BLES/menthol monolayer was then compressed quasi-statically at a rate of 0.05 cm<sup>2</sup>/min, i.e., 0.3 A%/s.

### Atomic Force Microscopy

To directly visualize the impact of ECAs on the PS film, we used atomic force microscopy (AFM) in conjunction with a newly developed subphase replacement technique for in situ Langmuir-Blodgett (LB) transfer in CDS (39). First, the surfactant vesicles in the aqueous subphase (i.e., the droplet) were replaced with an equal amount of buffer using a coaxial pedestal system without disturbing the adsorbed BLES film. Second, the BLES film was LB transferred by lifting a small piece of freshly peeled mica sheet across the air-water surface at a speed of 1 mm/min. Third, topographical images of the immobilized BLES films were acquired with an Innova AFM (Bruker, Santa Barbara, CA), with the tapping mode scan using a silicon cantilever with a resonance frequency of 300 kHz and a spring constant of 42 N/m. Each sample was scanned at multiple locations to ensure representativeness and reproducibility. AFM images were analyzed using the Nanoscope Analysis software (version 1.5).

### <sup>13</sup>C-Nuclear Magnetic Resonance

BLES (10 mM) was mixed with menthol at a molar ratio of 1:1 in deuterated chloroform. <sup>13</sup>C-nuclear magnetic resonance (<sup>13</sup>C-NMR) spectra were recorded using a Varian Unity INOVA 500 MHz NMR spectrometer, equipped with a pulse-field gradient module (z-axis) using a 5 mm switchable broadband probe at 125.76 MHz. The <sup>13</sup>C chemical shifts were reported relative to deuterated chloroform at 77.0 ppm as the internal standard.

### Circular Dichroism

A Chirascan V100 spectrophotometer (Applied Photophysics, Leatherhead, UK) was used to conduct circular dichroism (CD) measurements of BLES/menthol mixtures at different molar ratios. Samples were placed in a 10-mm path length cell. Protein secondary structure of BLES in various menthol concentrations was monitored between 200 and 260 nm. Each sample was measured three times. Background contributions from the solvent, menthol, and lipids were removed by subtracting appropriate buffer controls.

### Molecular Dynamics Simulations

The all-atom molecular dynamics (MD) system contains two symmetric monolayers separated by TIP3 water, as shown in Supplemental Fig. S1 (all Supplemental material is available at <https://doi.org/10.6084/m9.figshare.18517247.v1>). Periodic boundary conditions are enforced in all three directions. The model PS film consists of dipalmitoyl phosphatidylcholine (DPPC) and palmitoyl-oleoyl phosphatidylglycerol (POPG) at a molar ratio of 7:3. The initial configuration of the model PS film was generated with the

CHARMM-GUI membrane builder (40). The coordinates for menthol were obtained from the ZINC database (41). Each monolayer contained 35 DPPC and 15 POPG, separated by 4,086 TIP3 water molecules. Forty ions of  $K^+$  and 10 ions of  $Cl^-$  were added to mimic the physiological concentration of 0.15 M and to neutralize the total charge of the system. The length of the vacuum separating the two monolayers was roughly 30 nm (Supplemental Fig. S1) to eliminate all possible interactions between the two monolayers. Steepest descent energy minimization was carried out, followed by an equilibration under a canonical (NVT) ensemble, both utilizing position restraints on menthol and lipids. During the equilibration, menthol, lipids, and water molecules were coupled to separate temperature baths, maintained at 310 K using the Berendsen thermostat. The system was then equilibrated under NPT conditions using the Nose-Hoover thermostat and Parrinello-Rahman barostat with semi-isotropic coupling at 1 bar. The volume of the system, with a box dimension of  $5.59 \times 5.59 \times 40.0$  nm, was chosen to maintain a constant surface pressure corresponding to  $\sim 40$  mN/m. Further equilibration was run for 100 ns in the absence of restraints, under an NVT ensemble using the Nose-Hoover thermostat. The equilibration structure was used as a starting point to prepare structures for umbrella sampling. The relative distance between the center-of-mass (COM) of menthol and the COM of the system is defined as the “COM distance.” The initial COM distance was set at 0.0, meaning that menthol starts in the center of the water box (Supplemental Fig. S1). The COM distance of  $\sim 2.0$  nm indicates that menthol is near the headgroups of the phospholipids and the COM distance of  $\sim 4.0$  nm indicates that menthol is near the edge of the tail groups of the phospholipids. Further increase of COM distance indicates that menthol is transiting out of the monolayer into the vacuum. The “pull” function in GROMACS-2019.1 (42) was employed to prepare initial configurations for a series of MD simulations, i.e., “windows” of umbrella sampling, where menthol was placed at different COM distances, initiated from the center of the water box, i.e., COM distance of 0.0 nm, and ended in vacuum, i.e., COM distance of  $\sim 5.6$  nm. Different COM distances were used to generate windows along the Z direction (Supplemental Fig. S1). A window was generated every 0.02 nm between COM distances 0.0 and 3.0 nm, whereas every 0.05 nm for larger COM distances. A harmonic potential with a spring constant of  $1,000$  kJ/mol/nm<sup>2</sup> was employed to ensure menthol stays at its respective COM distance for 40 ns, where the first 20 ns are considered equilibration and the last 20 ns are used for the umbrella window. A total time of 8,160 ns, corresponding to 204 umbrella windows, was simulated and the overlap between adjacent windows was ensured (Supplemental Fig. S2). The free energy of the system with respect to the relative position of menthol was analyzed with the weighted histogram method (WHAM) (43) and the error bars were compared with the bootstrapping method (44).

### Statistical Analysis

Data in each group are shown as means  $\pm$  standard deviation ( $n = 5$ , unless otherwise noted). Shapiro-Wilk test (OriginPro, Northampton, MA) was performed to confirm

normality of data in each group. One-way ANOVA together with the Tukey means comparison test (OriginPro) were used to determine group differences.  $P < 0.05$  was considered statistically significant.

## RESULTS

### ECA-Induced Biophysical Inhibition

We first studied the effect of ECA exposure dose on the BLES film under physiologically relevant conditions, i.e., 37°C and 100% relative humidity, using the combination of CDS and a home-made ECA generator, as illustrated in Fig. 1. As shown in Supplemental Fig. S3, the ECA generator can produce and deliver reproducible amounts of aerosols into the CDS chamber,  $\sim 10$  mg per puff. This aerosol mass per puff produced with our ECA generator fell into the general range of aerosol yield by e-cigarette devices, i.e., 1.5–28 mg per puff (45). This aerosol mass per puff corresponds to an aerosol concentration of  $\sim 25$   $\mu\text{g}/\text{cm}^3$  in the controlled environment. As shown in Supplemental Fig. S4, exposure to 3 puffs, 15 puffs, and 30 puffs of aerosols, generated from a commercial menthol-flavored e-liquid, increases the  $\gamma_{\text{min}}$  of BLES from less than 3 mN/m to 4.6, 6.3, and 8.8 mN/m, respectively. The  $\kappa_{\text{comp}}$  of the BLES film is also increased from 0.64 to 0.97 m/mN after exposure to 30 puffs of the aerosols, indicating significant surfactant inhibition. We thereafter use 30 puffs as a representative dose of ECA exposure.

Figure 2, A–C, shows the effect of individual chemical components of the commercial menthol-flavored e-liquid on BLES. Exposure to aerosols of the vehicle solvent alone, i.e., propylene glycol (PG) and vegetable glycerin (VG; vol/vol, 50/50), only slightly elevates the  $\gamma_{\text{min}}$  and  $\kappa_{\text{comp}}$  of BLES to 4.8 mN/m and 0.76 m/mN, respectively. Addition of 6 mg/mL nicotine alone does not significantly change the results of the solvent. However, adding 12 mg/mL menthol significantly increases  $\gamma_{\text{min}}$  and  $\kappa_{\text{comp}}$  to 6.8 mN/m and 0.92 m/mN, respectively. The fully recombinant e-liquid, i.e., 6 mg/mL nicotine and 12 mg/mL menthol dissolved in PG/VG, demonstrates a similar inhibition effect compared to the commercial e-liquid. These results demonstrate that menthol is likely to be the major chemical component in the e-liquid causing biophysical inhibition of PS.

Figure 2, D–F, shows the effect of menthol, and two other popular flavor chemicals, i.e., ethyl maltol and ethyl butyrate, on BLES. Menthol increases the  $\gamma_{\text{min}}$  of BLES from  $\sim 3.5$  to  $\sim 6.5$  mN/m, whereas ethyl maltol and ethyl butyrate only increase the  $\gamma_{\text{min}}$  to  $\sim 4.5$  mN/m. Hence, it appears that menthol causes more biophysical inhibition of BLES than ethyl maltol or ethyl butyrate does. Similar conclusions can be drawn from the film compressibility analysis. Menthol increases the  $\kappa_{\text{comp}}$  of BLES film by 30% whereas ethyl maltol and ethyl butyrate only increase the  $\kappa_{\text{comp}}$  of BLES by 10% and 6%, respectively. Figure 2, G–I, shows the effect of these flavor chemicals, plus nicotine, on BLES. It appears that the addition of nicotine does not significantly vary the degree of biophysical inhibition, thus reasserting that the flavorings, especially menthol, play a predominant role in inhibiting the biophysical function of PS. Reproducibility of all

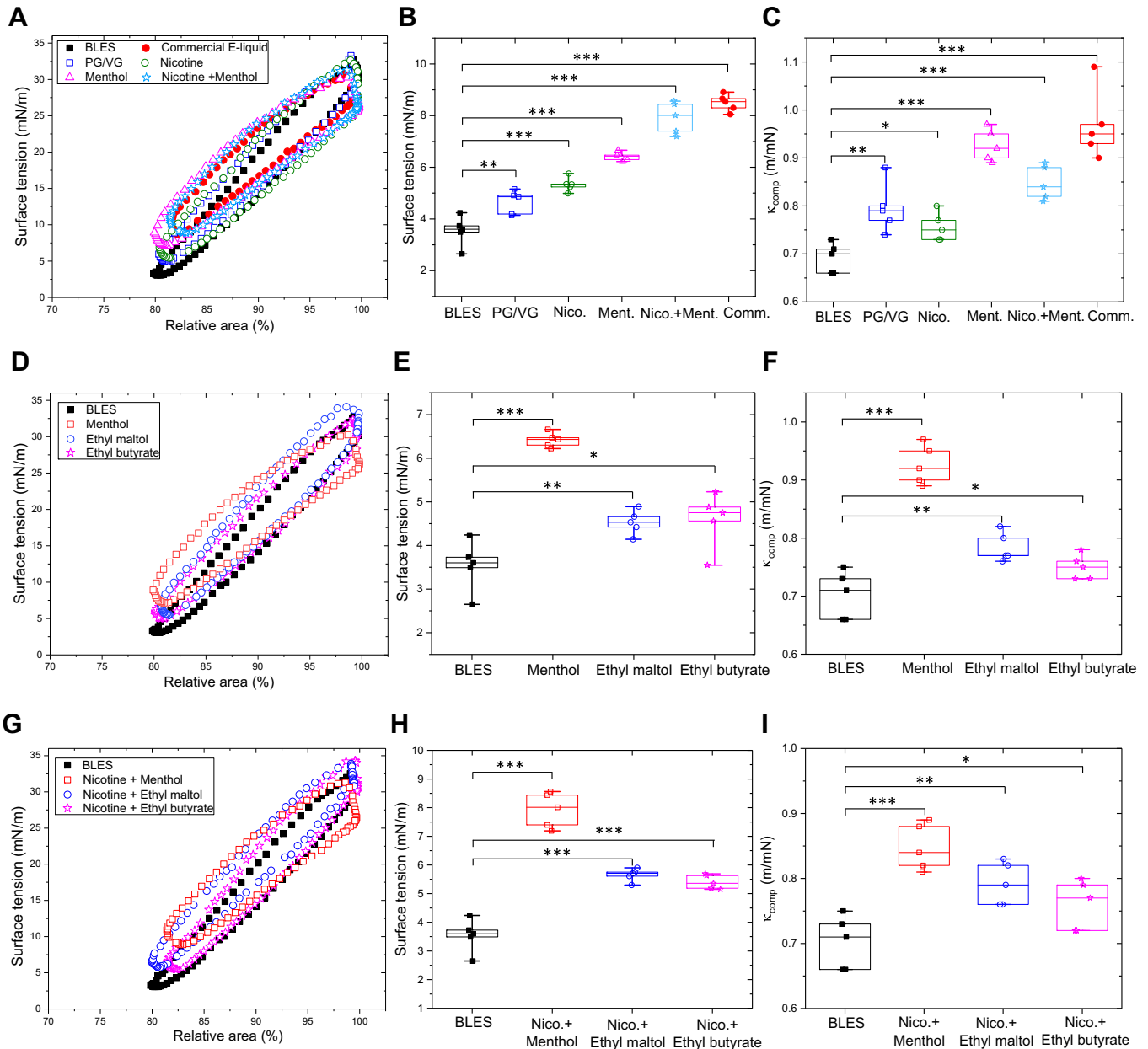


**Figure 2.** Effect of e-liquid chemical components on the biophysical properties of a natural surfactant, BLES, after exposure to 30 puffs of ECAs. A–C: effect of a commercial e-liquid, and the recombinant e-liquids, including the solvent PG/VG (1:1), PG/VG + nicotine, PG/VG + menthol, and PG/VG + nicotine + menthol, on BLES. A: dynamic compression-expansion cycles (i.e., simulation of respiratory cycles) of BLES before and after exposure to ECAs. B and C: statistical analysis of the minimum surface tension ( $\gamma_{min}$ ) and film compressibility ( $K_{comp}$ ), respectively. D–F: effect of individual flavor chemicals, i.e., menthol (12 mg/mL), ethyl maltol (10 mg/mL), and ethyl butyrate (7.4 mg/mL), on BLES. G–I: effect of individual flavors plus nicotine (6 mg/mL) on BLES. All data ( $n = 5$ ) of ECA exposure show statistically significant differences in comparison to the BLES film without exposure to aerosols; \* $P < 0.05$ , \*\* $P < 0.01$ , and \*\*\* $P < 0.001$ . BLES, bovine lipid extract surfactant; ECAs, electronic cigarette aerosol; PG, propylene glycol; VG, vegetable glycerin.

dynamic cycling experiments can be found in Supplemental Fig. S5.

### Directly Imaging the Effect of ECA Exposure on the PS

Figure 3 shows lateral structure and topography of the BLES film before and after exposure to the aerosols. Reproducibility of the AFM images can be found in Supplemental Fig. S6. As shown in Fig. 3A, the adsorbed BLES film demonstrates a uniformly distributed multilayer structure

with protrusions  $\sim 22$  nm in height, corresponding to 5–6 stacked phospholipid bilayers, given the thickness of a fully hydrated phospholipid bilayer at  $\sim 4$  nm. After exposure to the commercial menthol-flavored ECAs (Fig. 3B) and fully recombinant ECAs (Fig. 3C), the conformation of the BLES film is dramatically changed from a multilayer (featuring multilayered protrusions  $>4$  nm) to a monolayer (featuring solid-like domains  $\sim 1$  nm higher than the surrounding fluid-like domains). It was found that exposure to aerosols that

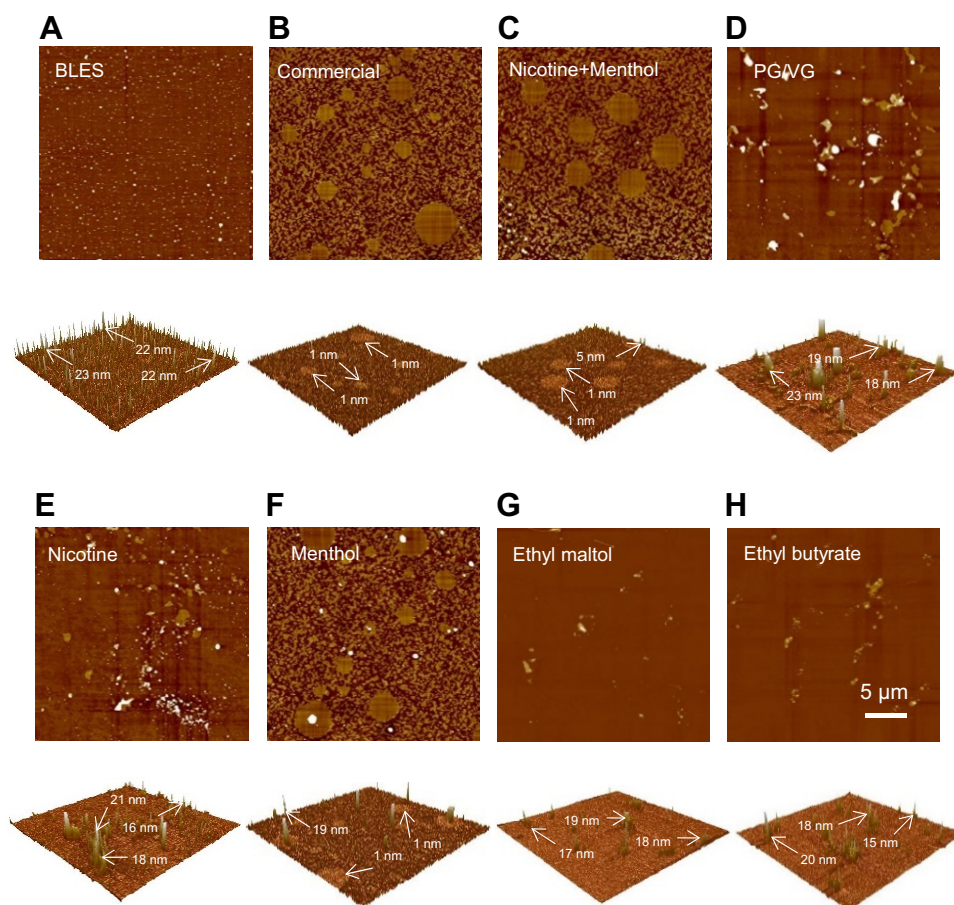


**Figure 3.** Effect of e-liquid chemical components on the lateral structure and topography of the BLES film (A), and the BLES film exposed to 30-puff aerosols of a commercial menthol-flavored e-liquid containing 6 mg/mL nicotine (B), or fully recombinant e-liquids, including the solvent of PG/VG, nicotine, and menthol (C). D–H: effect of ECAs of individual chemical components on the BLES film, including PG/VG (D), 6 mg/mL nicotine (E), 12 mg/mL menthol (F), 10 mg/mL ethyl maltol (G), and 7.4 mg/mL ethyl butyrate (H). All AFM images were obtained at the equilibrium surface tension ( $\gamma_e$ ) and have the same scanning area of  $20 \times 20 \mu\text{m}$ . All images are shown in both 2-D topography and 3-D rendering. The z range for images exposed to three menthol-containing ECAs is 5 nm, and the z range for the rest images is 20 nm. White arrows denote the height measurements in the AFM images. BLES, bovine lipid extract surfactant; ECAs, electronic cigarette aerosol; PG, propylene glycol; VG, vegetable glycerin.

contain only the solvent (Fig. 3D), or nicotine (Fig. 3E) reduces the amount of multilayered protrusions but not completely remove them from the BLES film. However, exposure to aerosols that contain only menthol causes the multilayer-to-monolayer degradation (Fig. 3F), similar to exposure to the commercial menthol-flavored ECAs (Fig. 3B) or the fully recombinant ECAs (Fig. 3C), thus indicating that menthol is the primary chemical compound in ECAs to cause biophysical inhibition of BLES. Figure 3, G and H, shows the effect of ethyl maltol and ethyl butyrate on the BLES film, respectively. These two flavor chemicals disturb the BLES film by reducing the amount of multilayer structures but not completely removing them, as menthol does.

### Molecular Interactions between Menthol and Surfactant Phospholipids and Proteins

We have scrutinized the molecular mechanism by which menthol inhibits the biophysical function of natural PS. Figure 4A shows the quasi-static isothermal compression of a BLES monolayer. The BLES monolayer was exposed to menthol in two different ways, i.e., directly cospreading with menthol in 10:1 and 1:1 molar ratios, or exposure to aerosols generated with the menthol-containing (12 mg/mL) e-liquid. Reproducibility of the compression isotherms can be found in Supplemental Fig. S7. The compression isotherm of menthol is also included as a negative control. Exposure to menthol, either in aerosols or directly added to the BLES monolayer, inhibits the monolayer-to-multilayer transition

of the BLES film; i.e., the surface pressure does not increase beyond the transition plateau at  $\sim 50 \text{ mN/m}$ . Such inhibition cannot be explained by competitive adsorption since menthol alone demonstrates only moderate surface activity.

Figure 4B shows the lateral structure of the spread BLES film, before and after exposure to menthol, at four representative surface pressures of 20, 30, 40, and 50 mN/m, respectively. Reproducibility of the AFM images can be found in Supplemental Figs. S8–S11. Quantification results of the phospholipid domain size are shown in Fig. 4C. Menthol significantly reduces the size of solid-like domains of the BLES monolayer. For instance, exposure to menthol-containing ECAs reduces the domain size of BLES at 30 mN/m from  $\sim 4.7$  to  $<1 \mu\text{m}$ , indicating direct disturbance of phospholipids in BLES. All BLES monolayers exposed to menthol, either in aerosols or directly added to the BLES monolayer, are incapable of transforming into multilayers at 50 mN/m, indicating disturbance of surfactant-associated proteins, SP-B and/or SP-C in BLES. These results indicate that menthol likely inhibits the PS by specifically interacting with both phospholipids and proteins in PS.

To study the specific molecular interactions between menthol and phospholipids and proteins in BLES, we have performed  $^{13}\text{C}$ -NMR and CD measurements. Figure 5, A and B, shows the chemical shift of representative  $^{13}\text{C}$ -NMR spectra of BLES due to the addition of menthol at 1:1 molar ratio. The largest chemical shift caused by menthol is found at carbon atoms in the headgroups of the phospholipids,

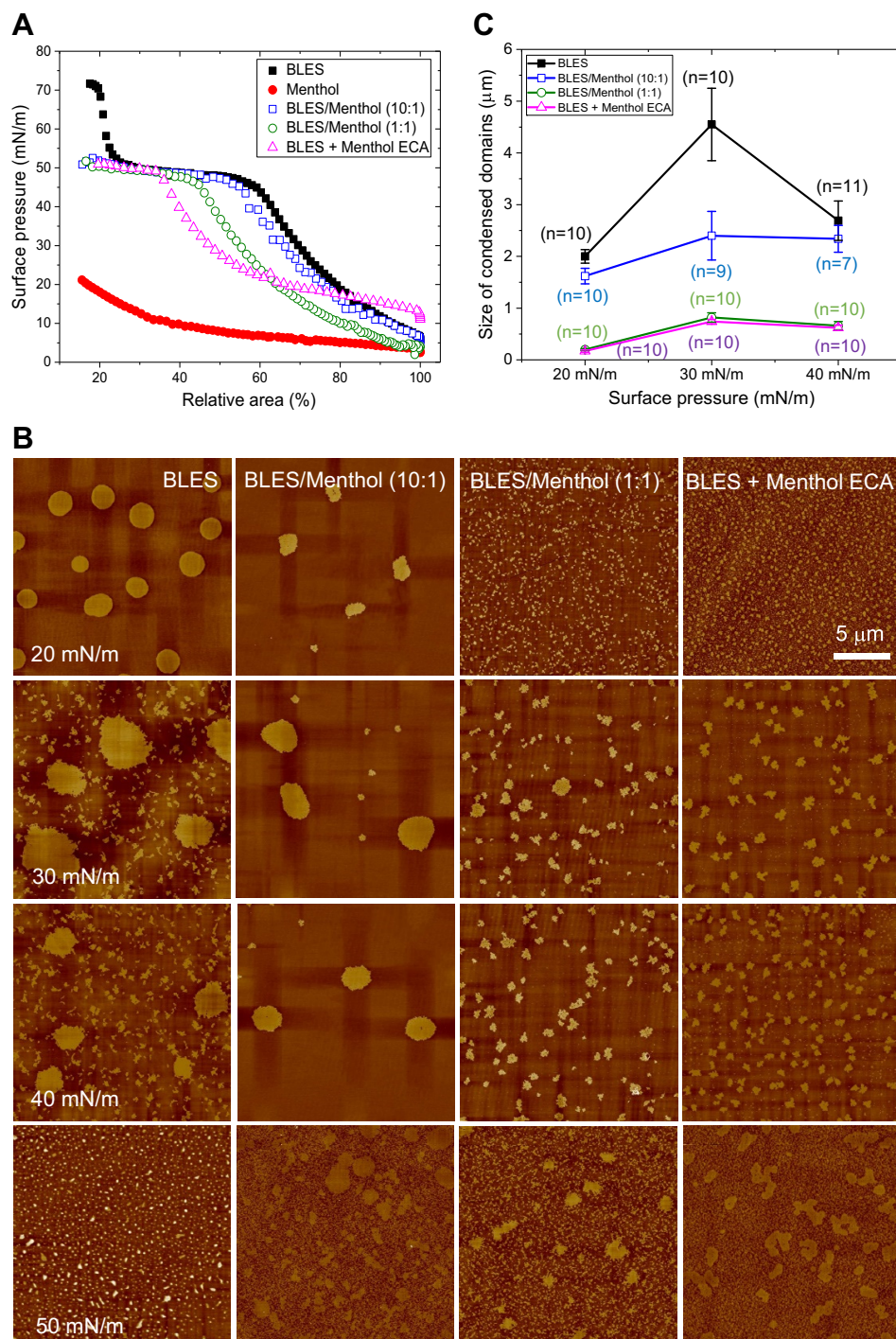


**Figure 4.** Effect of menthol on the quasi-static surface activity of BLES. **A:** compression isotherms of BLES (as a positive control), menthol (as a negative control), BLES/menthol mixtures at molar ratios of 10:1 and 1:1, and BLES after exposure to 30-puffs menthol ECAs. Biophysical inhibition of BLES by menthol is indicated by decreases in the collapse surface pressure ( $\pi_c$ ). **B:** lateral structure and molecular organization of the BLES with/without addition of menthol, at four representative surface pressures of 20, 30, 40, and 50 mN/m, respectively. All the images have the same scanning area of  $20 \times 20 \mu\text{m}$ . The z range is set to be 5 nm for all the images except 20 nm for the image of BLES at 50 mN/m. **C:** quantification results of the size of condensed domains in the BLES monolayer, with/without menthol, at 20, 30, and 40 mN/m, respectively. The  $n$  number for individual data point is shown in the figure. All data of the BLES film exposed to menthol show statistically significant differences ( $P < 0.001$ ) in comparison to the BLES film, except for BLES/Menthol (10:1) at 40 mN/m, for which  $P = 0.052$ . BLES, bovine lipid extract surfactant; ECAs, electronic cigarette aerosol.

especially at the  $\gamma$  and  $\beta$  locations. It should be noted that the most significant chemical shifts at these locations are only 0.05 ppm, likely due to the low BLES concentration (10 mM) used for the measurements. CD is a highly sensitive analytical technique that probes the secondary structure of a protein using the effect of chirality on circular polarized light. CD spectral shifts are indicative of loss of the secondary structure and/or changes between  $\alpha$ -helical and  $\beta$ -strand structures. Figure 5C shows the CD spectra of BLES and menthol at three molar ratios: 100:1, 10:1, and 1:1. The spectra for BLES, without adding menthol, shows typical  $\alpha$ -helical

spectra with minima at 208 and 222 nm, indicating the helical secondary structures of SP-B and/or SP-C in BLES (46, 47). Tashiro et al. (47) showed that SP-C exists both as a monomer and a dimer depending on the protein concentration. Our results at low menthol concentrations (100:1) show a small change in CD signal between 200 and 240 nm, which may indicate dimer dissociation of SP-B and/or SP-C. At high menthol concentrations (10:1 and 1:1), there are significant spectral changes from a helical to a more  $\beta$ -like structure, indicating loss of the helical structure of SP-B and/or SP-C (48). Therefore, the CD measurements

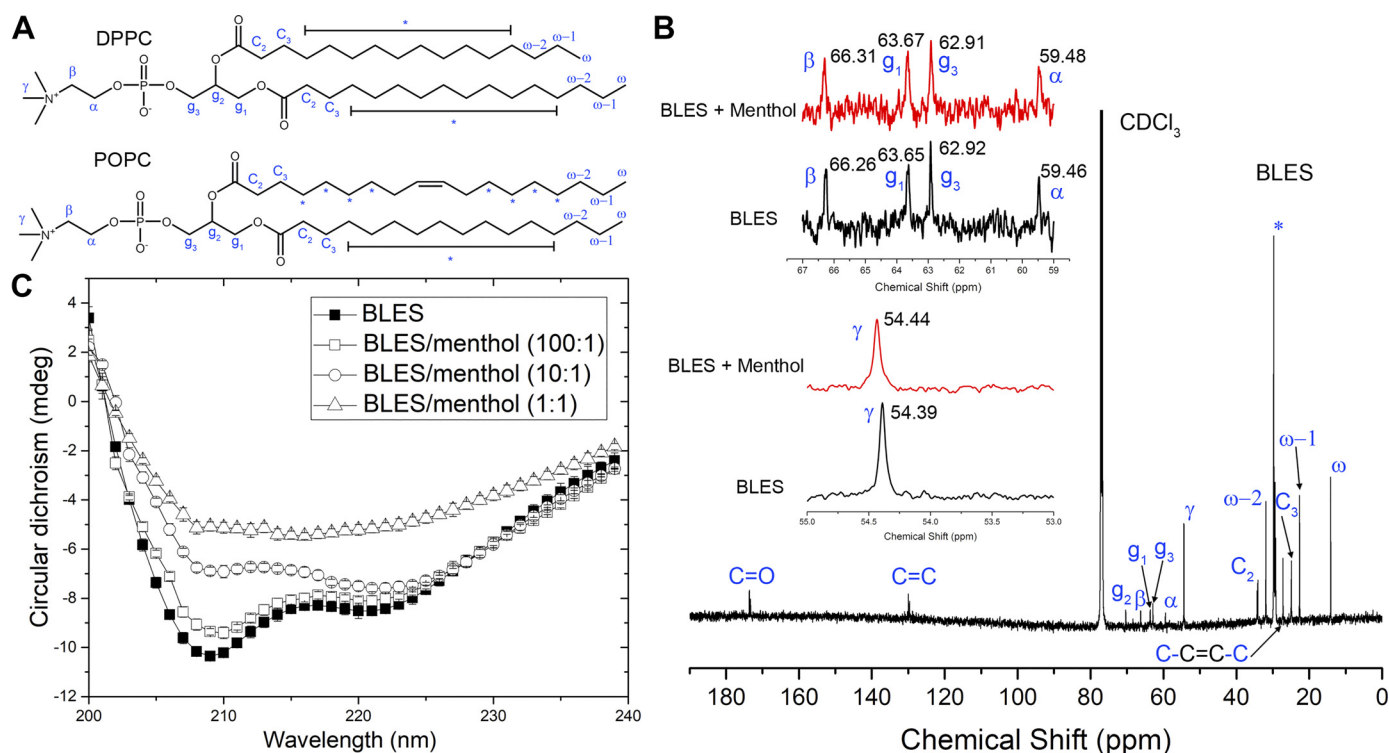


**Figure 5.** Molecular interactions between menthol and surfactant phospholipids and proteins. **A:** labels denoted to distinct segments of representative phospholipids in natural PS, i.e., dipalmitoyl phosphatidylcholine (DPPC) and palmitoyl-oleoyl phosphatidylcholine (POPC). **B:** a  $^{13}\text{C}$ -NMR spectrum of BLES with peak assignments of phospholipid acyl chains and headgroups. *Insets* show chemical shifts, due to the addition of menthol, at carbon atoms labeled as  $\alpha$ ,  $\beta$ ,  $\gamma$ ,  $g_1$ , and  $g_3$ . The NMR measurements were carried out with deuterated chloroform solutions of BLES or BLES/menthol complex at a constant BLES concentration of 10 mM at room temperature. **C:** circular dichroism (CD) spectra of BLES and BLES/menthol mixtures at molar ratios of 100:1, 10:1, and 1:1, respectively. The CD measurements were conducted with a constant BLES concentration of 1 mg/mL at 25°C. BLES alone shows a typical  $\alpha$ -helical protein spectrum with two minima at 208 and 222 nm. Addition of menthol significantly disrupts the native conformation of surfactant proteins in BLES, indicated by decreased  $\alpha$ -helicity of the CD spectra. BLES, bovine lipid extract surfactant; PS, pulmonary surfactant.

provide direct evidence of surfactant protein denaturation due to menthol.

### MD Simulation of Menthol-Phospholipid Interactions

Figure 6 shows the MD simulation of specific interactions between menthol and a model PS monolayer of DPPC/POPG (7:3). Figure 6A shows the free energy profile of menthol interaction with the model PS monolayer at the air-water surface. The minimum of the free energy profile (point *b* in Fig. 6A) indicates that menthol prefers to interact with carbon atoms located at the junction between the headgroup and tail of the phospholipid. This favored position bespeaks for a potential of menthol to alter the surface activity and lipid domain formation in the PS monolayer.

Structural analysis was performed on selected umbrella windows to further elucidate the mechanism of interactions between menthol and the phospholipid monolayer at different center-of-mass (COM) distances. We have studied interactions at three characteristic COM distances, labeled as points *a*, *b*, and *c* in Fig. 6A. Point *a* (1.43 nm) refers to a location near the air-water surface where the phospholipid headgroups are located. Point *b* (2.68 nm) refers to a location at the junction between the phospholipid headgroup and tail, and point *c* (4.07 nm) refers to a location where the phospholipid tails meet vacuum. Figure 6B demonstrates the distribution of the angle between the hydroxyl of menthol and z-

axis defined in Fig. 6C, of which the angular entropy has been taken into account and scaled properly. As shown in Fig. 6A, menthol preferably partitions into the phospholipid monolayer at the junction between the headgroup and tail (point *b*), at which the hydrophilic hydroxyl group orients itself toward the phospholipid headgroup while leaving the hydrophobic moiety of menthol in the tail. This orientation maximizes the electrostatic interaction between the phospholipid and menthol, resulting a significant free energy minimum.

## DISCUSSION

Being a main attraction to e-cigarette users, especially youth, flavorings have become the major ingredient of e-cigarette products. Although most flavorings used in e-cigarettes are food-grade additives and scents, their safety and health impact on the respiratory system, at levels inhaled by e-cigarette users, are largely unknown (10). Many recent *in vitro* and *in vivo* studies have raised substantial concerns about the toxicity of e-cigarette flavorings, including cytotoxicity, immunotoxicity, and the potential of triggering proinflammatory responses (6, 7, 12, 49).

As of 2018, there were more than 15,000 different e-cigarette flavor blends available on the market (50). Krüsemann et al. (51) have classified these flavors into 13 main categories,

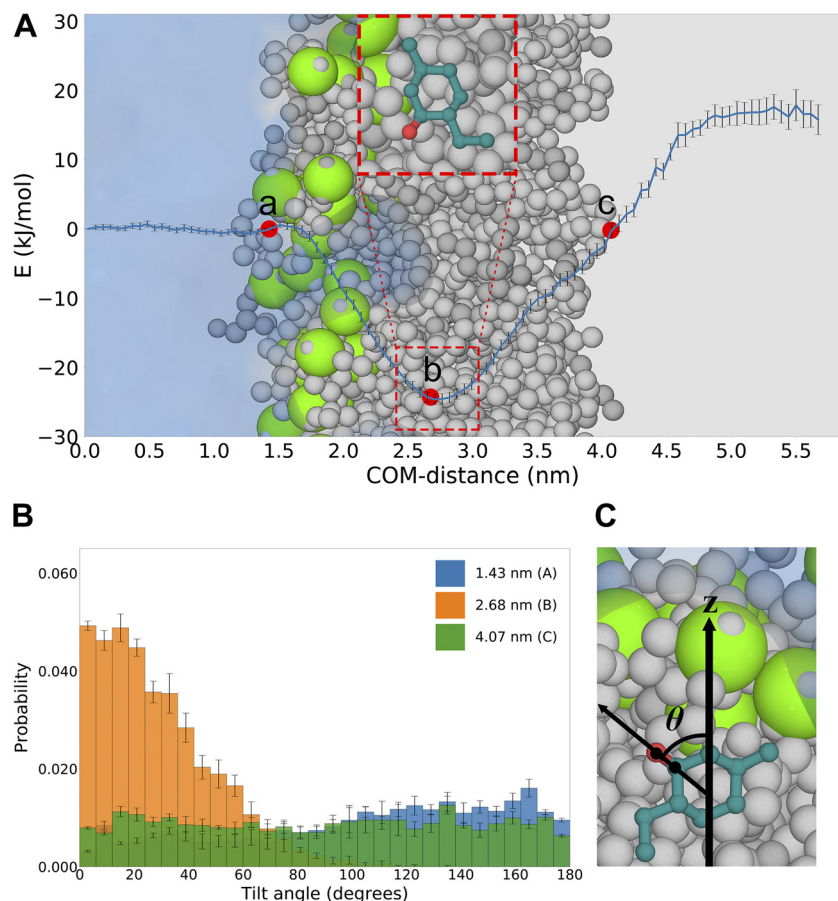


**Figure 6.** MD simulation of menthol-phospholipid interactions. **A:** a demonstration of the all-atom MD system. Green spheres represent the phosphorus atoms in the headgroup of the phospholipids, gray spheres represent the tail group of the phospholipids, and water is represented as a transparent blue phase between the monolayers. The vacuum extends  $\sim 15$  nm to the left and to the right of the monolayer tails (Supplemental Fig. S1). Overlay is a one-dimensional, center-of-mass (COM) distance, free energy profile of interactions between menthol and the phospholipid monolayer. The three points (a–c) represent menthol at different COM distances. The COM distance *b* at the free energy minimum is highlighted in a red box to demonstrate the preferred orientation of menthol. **B:** angular distributions of menthol partitioned at different COM distances as depicted in **A**. Distributions are taken as averages over two nearest windows. **C:** definition of the angle between menthol and the norm of the phospholipid (*z* direction). MD, molecular dynamics.

including tobacco, menthol, fruit, dessert, alcohol, nut, spices, candy, coffee/tea, beverages, sweet-like flavors, unspecified flavors, and unflavored e-liquids. Commercially, each of these flavors is made of combinations of various flavor chemicals at various concentrations, with a total of flavor chemicals in the 1–4 wt% (i.e., 10–40 mg/mL) range of the e-liquid (2, 52). Among all these flavor chemicals, it was found that vanillin, ethyl maltol, and ethyl butyrate are the top three chemical ingredients used in all commercial e-cigarette products (2, 52). Menthol is the major chemical ingredient of the menthol/mint flavored e-cigarette. It is among the top 20 most frequently added flavor chemicals in e-cigarette products (52) and is usually used with a concentration much higher than other flavor chemicals (2, 52, 53), for example, at a concentration as high as 84 mg/mL (54).

Menthol is a naturally occurring cyclic terpene alcohol of plant origin (55). It is a commonly used penetration enhancer for topical drug administration in dermatology. The specific molecular mechanism by which menthol enhances membrane penetration is not yet completely understood, but disturbing lipid packing in the membrane structure of the stratum corneum is considered to be an important contributor (56). Direct NMR evidence exists for menthol penetrating into the hydrophilic headgroups of a model biomembrane (57). Early *in vivo* experiments suggested that long-term inhalation of tobacco smoke with a low menthol concentration of 5 mg/mL caused no substantial adverse effect on rats (58). However, very recent multiplatform studies have demonstrated that

acute exposure to menthol-containing ECAs adversely affected human bronchial epithelium in a manner that could lead to respiratory disease (59).

Our study shows that ECAs with three flavor chemicals at typical concentrations used in commercial e-cigarette products, i.e., menthol (12 mg/mL), ethyl maltol (10 mg/mL), and ethyl butyrate (7.4 mg/mL), all demonstrate a deleterious effect on the biophysical function of BLES, an animal-derived natural PS (Fig. 2). Among all three chemicals, menthol shows the most adverse biophysical impact, indicated by increases in the minimum surface tension and film compressibility. We also found that nicotine alone (6 mg/mL) only moderately affects the biophysical function of BLES (Fig. 2). Nicotine concentration used in e-liquid can vary greatly from 0 to  $>50$  mg/mL, and there is a trend of increasing sale of e-liquid containing very high nicotine concentrations ( $\geq 50$  mg/mL) (60). As such, the nicotine concentration studied here represents the low-end concentration used in commercial e-cigarettes. At this low nicotine concentration, we found that the deleterious effect of flavor chemicals is relatively independent from nicotine (Fig. 2), whereas future studies are needed to assess the impact of different forms (such as nicotine salts) and concentrations of nicotine on surfactant. This finding is qualitatively consistent with the recent report that chronic exposure to ECAs cause alternation of lipid homeostasis in alveolar macrophages and epithelial cells, and such alternations were found to be independent of nicotine (14). Our biophysical studies suggest

that flavor chemicals, especially menthol, are the major chemical compound in ECAs to inhibit the biophysical function of PS.

This biophysical finding is supported by directly imaging the effect of ECA exposure on the BLES film using AFM (Figs. 3 and 4). It is found that exposure to three menthol-containing ECAs, i.e., the commercial menthol-flavored e-liquid (Fig. 3B), the recombinant e-liquids containing menthol and nicotine (Fig. 3C), and menthol alone (Fig. 3F), completely inhibits the monolayer-to-multilayer transition of the BLES film. Transition from a monolayer to uniformly distributed multilayers under extreme lateral compression is characteristic attributes of a healthy PS (26, 39, 61). Impairment of the monolayer-to-multilayer transition is a strong indication of surfactant inhibition associated with dysfunction of SP-B and/or SP-C (62–64), since these hydrophobic proteins play a key role in stabilizing the negative-curvature required to stabilize the multilayers (65–67). In line with the AFM observation, our CD measurements have provided direct evidence of menthol interactions with SP-B and/or SP-C, as indicated by a change of secondary structure from  $\alpha$ -helical to a more  $\beta$ -like structure (Fig. 5C). It appears that this protein denaturation due to menthol is significant enough to destabilize the multilayer structure essential for a healthy PS.

In addition to interactions with surfactant-associated proteins, our data suggest that menthol also disturbs the phospholipids in BLES. It is found that menthol in aerosols or directly added to the BLES monolayer significantly reduces the size of solid-like phospholipid domains in the BLES monolayer (Fig. 4). The fact that either exposure to menthol-containing ECAs or directly adding menthol to the BLES monolayer induces a similar degree of surfactant inhibition indicates that menthol does not go through significant chemical pyrolysis during the vaporization process. One source of ECA toxicity is believed to be the formation of chemically unstable pyrolysis products of flavors and/or vehicle solvents during vaporization of the e-liquid, typically occurring at the temperature range between 100°C and 250°C (6, 68, 69). However, menthol is relatively stable in this temperature range (70). It was found that menthol has a relatively high, closely to 100%, transfer efficiency from the e-liquid to aerosols (54). Our findings are consistent with those reported by Nair et al. (59), who found that exposure to menthol in ECAs or directly added to cell cultures induces a similar degree of cytotoxicity as manifested by different *in vitro* models.

The phospholipid domain size depends on a balance between the line tension and electrostatic repulsion between phospholipid headgroups (26). The change of domain morphology therefore indicates direct interactions between menthol and phospholipid headgroups, which alter the intermolecular force balance at the domain boundaries. This hypothesis is supported by  $^{13}\text{C}$ -NMR measurements that show chemical shifts of carbons around the phospholipid headgroup caused by menthol (Fig. 5B), and molecular dynamics simulations (Fig. 6), which directly manifest molecular interactions between menthol and phospholipids. Free energy calculations of our MD simulations support the following menthol-phospholipid interaction mechanism. Menthol is most likely partitioned into the phospholipid just beneath the phospholipid headgroup, leaving the hydroxyl group pointing toward bulk water and the rest hydrophobic part of

the molecule buried in the phospholipid tails. This interaction between menthol and phospholipids is very stable, and the corresponding position of menthol, as indicated in Fig. 6A, implies its potential of inhibiting the biophysical function of PS.

Menthol is the last and only flavor that is allowable in combustible cigarettes marketed in the United States under the 2009 Family Smoking Prevention and Tobacco Control Act. On April 29, 2021, the US Food and Drug Administration (FDA) made an announcement to ban menthol in all cigarettes and flavored cigars within a year. If the ban were enforced, research predicts that up to 30% of current menthol cigarette smokers would switch to e-cigarettes (71). This would quickly expand the market of menthol-flavored e-cigarettes. Our results show that there is an urgent need to better understand the health impact of menthol-flavored e-cigarettes, which may contribute to a better regulation of e-cigarette products.

It is important to restate two major limitations of the present study. First, we only studied one vaping device, which is a third-generation modifiable e-cigarette device with a sub-ohm tank. Further study is needed to verify whether the surfactant inhibitory effect found here is generalizable to other e-cigarette devices. Second, the present study only focused on the biophysical effect of e-cigarette aerosols on surfactant. We used an animal-derived clinical surfactant preparation, BLES, which is devoid of the hydrophilic surfactant proteins, SP-A and SP-D. SP-A and SP-D play a central role in innate host defense against inhaled pathogens and particles (72). A recent study by Madison et al. (14) found that long-term exposure to e-cigarette aerosols reduced the expression of surfactant proteins, thus likely disturbing both the biophysical and immunological functions of pulmonary surfactant.

In summary, using combined biophysical assessments, AFM imaging,  $^{13}\text{C}$ -NMR, CD spectroscopy, and *in silico* MD simulations, we have concluded that menthol used in e-cigarettes plays a predominant role in inhibiting the biophysical function of natural PS. The mechanism of biophysical inhibition appears to involve menthol interactions with both phospholipids and proteins, which disturb phospholipid packing and impair formation of PS multilayers. These findings provide a novel insight into the understanding of health impact of e-cigarettes.

## DATA AVAILABILITY

The data that support the findings of this study will be made available upon reasonable request from the corresponding author.

## SUPPLEMENTAL DATA

Supplemental Figs. S1–S11: <https://doi.org/10.6084/m9.figshare.18517247.v1>.

## ACKNOWLEDGMENTS

We thank Dr. Harold Nigh of BLES Biochemicals Inc. for donation of BLES samples.

Present addresses: L. Xu, State Key Laboratory of Solid Lubrication, Lanzhou Institute of Chemical Physics, Chinese Academy of Sciences, Lanzhou 730000, China; Y. Yang, State

Key Laboratory of Solid Lubrication, Lanzhou Institute of Chemical Physics, Chinese Academy of Sciences, Lanzhou 730000, China.

## GRANTS

This research was supported by the National Science Foundation Grant No. CBET-2011317 (to Y.Y.Z.) and the George F. Straub Trust and Robert C. Perry Fund of the Hawai'i Community Foundation Grant No. 18ADVC-90802 (to Y.Y.Z.).

## DISCLOSURES

No conflicts of interest, financial or otherwise, are declared by the authors.

## AUTHOR CONTRIBUTIONS

Y.Y.Z. conceived and designed research; L.X., Y.Y., J.M.S., and C.K. performed experiments; L.X., Y.Y., J.M.S., C.K., G.L., X.X., E.H., and R.S. analyzed data; G.L., X.X., E.H., R.S., and Y.Y.Z. interpreted results of experiments; L.X., Y.Y., J.M.S., C.K., G.L., X.X., and Y.Y.Z. prepared figures; Y.Y.Z. drafted manuscript; E.H., R.S., and Y.Y.Z. edited and revised manuscript; Y.Y.Z. approved final version of manuscript.

## REFERENCES

1. Grana R, Benowitz N, Glantz SA. E-cigarettes: a scientific review. *Circulation* 129: 1972–1986, 2014. doi:10.1161/CIRCULATIONAHA.114.007667.
2. Tierney PA, Karpinski CD, Brown JE, Luo W, Pankow JF. Flavour chemicals in electronic cigarette fluids. *Tob Control* 25: e10–e15, 2016. doi:10.1136/tobaccocontrol-2014-052175.
3. Harrell MB, Weaver SR, Loukas A, Creamer M, Marti CN, Jackson CD, Heath JW, Nayak P, Perry CL, Pechacek TF, Eriksen MP. Flavored e-cigarette use: characterizing youth, young adult, and adult users. *Prev Med Rep* 5: 33–40, 2017. doi:10.1016/j.pmedr.2016.11.001.
4. Glantz SA, Bareham DW. E-Cigarettes: use, effects on smoking, risks, and policy implications. *Annu Rev Public Health* 39: 215–235, 2018. doi:10.1146/annurev-publhealth-040617-013757.
5. Walley SC, Wilson KM, Winickoff JP, Groner J. A public health crisis: electronic cigarettes, vape, and JUUL. *Pediatrics* 143: e20182741, 2019. doi:10.1542/peds.2018-2741.
6. Khlystov A, Samburova V. Flavoring compounds dominate toxic aldehyde production during e-cigarette vaping. *Environ Sci Technol* 50: 13080–13085, 2016. doi:10.1021/acs.est.6b05145.
7. Klager S, Vallarino J, MacNaughton P, Christiani DC, Lu Q, Allen JG. Flavoring chemicals and aldehydes in e-cigarette emissions. *Environ Sci Technol* 51: 10806–10813, 2017. doi:10.1021/acs.est.7b02205.
8. Zhao D, Aravindakshan A, Hilpert M, Olmedo P, Rule AM, Navas-Acien A, Aherrera A. Metal/metalloid levels in electronic cigarette liquids, aerosols, and human biosamples: a systematic review. *Environ Health Perspect* 128: 36001, 2020.
9. Chun LF, Moazed F, Calfee CS, Matthay MA, Gotts JE. Pulmonary toxicity of e-cigarettes. *Am J Physiol Lung Cell Mol Physiol* 313: L193–L206, 2017. doi:10.1152/ajplung.00071.2017.
10. Gotts JE, Jordt S-E, McConnell R, Tarran R. What are the respiratory effects of e-cigarettes? *BMJ* 366: 15275, 2019 [Erratum in *BMJ* 367: 15980, 2019]. doi:10.1136/bmj.15275.
11. Qasim H, Karim ZA, Rivera JO, Khasawneh FT, Alshbool FZ. Impact of electronic cigarettes on the cardiovascular system. *J Am Heart Assoc* 6: e006353, 2017. doi:10.1161/JAHA.117.006353.
12. Lechasseur A, Morissette MC. The fog, the attractive and the addictive: pulmonary effects of vaping with a focus on the contribution of each major vaping liquid constituent. *Eur Respir Rev* 29: 200268, 2020. doi:10.1183/16000617.0268-2020.
13. Wills TA, Knight R, Williams RJ, Pagano I, Sargent JD. Risk factors for exclusive E-cigarette use and dual E-cigarette use and tobacco use in adolescents. *Pediatrics* 135: e43–e51, 2015. doi:10.1542/peds.2014-0760.
14. Madison MC, Landers CT, Gu B-H, Chang C-Y, Tung H-Y, You R, Hong MJ, Baghaei N, Song L-Z, Porter P, Putluri N, Salas R, Gilbert BE, Levental I, Campen MJ, Corry DB, Kheradmand F. Electronic cigarettes disrupt lung lipid homeostasis and innate immunity independent of nicotine. *J Clin Invest* 129: 4290–4304, 2019. doi:10.1172/JCI128531.
15. Lee H-W, Park S-H, Weng M-W, Wang H-T, Huang WC, Lepor H, Wu X-R, Chen L-C, Tang M-S. E-cigarette smoke damages DNA and reduces repair activity in mouse lung, heart, and bladder as well as in human lung and bladder cells. *Proc Natl Acad Sci USA* 115: E1560–E1569, 2018. doi:10.1073/pnas.1718185115.
16. Church JS, Chace-Donahue F, Blum JL, Ratner JR, Zelikoff JT, Schwartzer JJ. Neuroinflammatory and behavioral outcomes measured in adult offspring of mice exposed prenatally to E-cigarette aerosols. *Environ Health Perspect* 128: 47006, 2020. doi:10.1289/EHP6067.
17. Werner AK, Koumans EH, Chatham-Stephens K, Salvatore PP, Armatas C, Byers P, Clark CR, Ghinai I, Holzbauer SM, Navarette KA, Danielson ML, Ellington S, Moritz ED, Petersen EE, Kiernan EA, Baldwin GT, Briss P, Jones CM, King BA, Krishnasamy V, Rose DA, Reagan-Steiner S; Lung Injury Response Mortality Working Group. Hospitalizations and deaths associated with EVALI. *N Engl J Med* 382: 1589–1598, 2020. doi:10.1056/NEJMoa1915314.
18. Cherian SV, Kumar A, Estrada-Y-Martin RM. E-Cigarette or vaping product-associated lung injury: a review. *Am J Med* 133: 657–663, 2020. doi:10.1016/j.amjmed.2020.02.004.
19. Manigrasso M, Buonanno G, Fuoco FC, Stabile L, Avino P. Aerosol deposition doses in the human respiratory tree of electronic cigarette smokers. *Environ Pollut* 196: 257–267, 2015. doi:10.1016/j.envpol.2014.10.013.
20. Fuoco FC, Buonanno G, Stabile L, Vigo P. Influential parameters on particle concentration and size distribution in the mainstream of e-cigarettes. *Environ Pollut* 184: 523–529, 2014. doi:10.1016/j.envpol.2013.10.010.
21. Ingebretsen BJ, Cole SK, Alderman SL. Electronic cigarette aerosol particle size distribution measurements. *Inhal Toxicol* 24: 976–984, 2012. doi:10.3109/08958378.2012.744781.
22. Mikheev VB, Brinkman MC, Granville CA, Gordon SM, Clark PI. Real-time measurement of electronic cigarette aerosol size distribution and metals content analysis. *Nicotine Tob Res* 18: 1895–1902, 2016. doi:10.1093/ntr/ntw128.
23. Mulder HA, Patterson JL, Halquist MS, Kosmider L, Turner JBM, Poklis JL, Poklis A, Peace MR. The effect of electronic cigarette user modifications and e-liquid adulteration on the particle size profile of an aerosolized product. *Sci Rep* 9: 10221, 2019. doi:10.1038/s41598-019-46387-2.
24. Montagaud Y, Manzotti B, Chevrel S, Leclerc L, Sarry G, Clotagatide A, Pourchez J, Prévôt N. Aerosol regional deposition of electronic cigarette emissions using an original ex vivo respiratory model. *J Aero Sci* 151: 105633, 2021. doi:10.1016/j.jaerosci.2020.105633.
25. Zuo YY, Veldhuizen RA, Neumann AW, Petersen NO, Possmayer F. Current perspectives in pulmonary surfactant—inhibition, enhancement and evaluation. *Biochim Biophys Acta* 1778: 1947–1977, 2008. doi:10.1016/j.bbame.2008.03.021.
26. Zhang H, Fan Q, Wang YE, Neal CR, Zuo YY. Comparative study of clinical pulmonary surfactants using atomic force microscopy. *Biochim Biophys Acta* 1808: 1832–1842, 2011. doi:10.1016/j.bbame.2011.03.006.
27. Da Silva E, Vogel U, Hougaard KS, Pérez-Gil J, Zuo YY, Sørlø JB. An adverse outcome pathway for lung surfactant function inhibition leading to decreased lung function. *Curr Res Toxicol* 2: 225–236, 2021. doi:10.1016/j.crttox.2021.05.005.
28. Veldhuizen RAW, Zuo YY, Petersen NO, Lewis JF, Possmayer F. The COVID-19 pandemic: a target for surfactant therapy? *Expert Rev Respir Med* 15: 597–608, 2021. doi:10.1080/17476348.2021.1865809.
29. Valle RP, Wu T, Zuo YY. Biophysical influence of airborne carbon nanomaterials on natural pulmonary surfactant. *ACS Nano* 9: 5413–5421, 2015. doi:10.1021/acsnano.5b01181.

30. Yang Y, Wu Y, Ren Q, Zhang LG, Liu S, Zuo YY. Biophysical assessment of pulmonary surfactant predicts the lung toxicity of nanomaterials. *Small Methods* 2: 1700367, 2018. doi:10.1002/smt.201700367.
31. Aszyk J, Kubica P, Woźniak MK, Namiesnik J, Wasik A, Kot-Wasik A. Evaluation of flavour profiles in e-cigarette refill solutions using gas chromatography–tandem mass spectrometry. *J Chromatogr A* 1547: 86–98, 2018. doi:10.1016/j.chroma.2018.03.009.
32. Yu K, Yang J, Zuo YY. Automated droplet manipulation using closed-loop axisymmetric drop shape analysis. *Langmuir* 32: 4820–4826, 2016. doi:10.1021/acs.langmuir.6b01215.
33. Brown CJ, Cheng JM. Electronic cigarettes: product characterisation and design considerations. *Tob Control* 23 Suppl 2: ii4–ii10, 2014.
34. Cheng T. Chemical evaluation of electronic cigarettes. *Tob Control* 23: ii11–ii17, 2014. doi:10.1136/tobaccocontrol-2013-051482.
35. Behar RZ, Hua M, Talbot P. Puffing topography and nicotine intake of electronic cigarette users. *PLoS One* 10: e0117222, 2015. doi:10.1371/journal.pone.0117222.
36. Robinson R, Hensel E, Morabito P, Roundtree K. Electronic cigarette topography in the natural environment. *PLoS One* 10: e0129296, 2015. doi:10.1371/journal.pone.0129296.
37. Olmedo P, Navas-Acien A, Hess C, Jarmul S, Rule A. A direct method for e-cigarette aerosol sample collection. *Environ Res* 149: 151–156, 2016. doi:10.1016/j.envres.2016.05.008.
38. Bachofen H, Schurch S, Urbinelli M, Weibel E. Relations among alveolar surface tension, surface area, volume, and recoil pressure. *J Appl Physiol (1985)* 62: 1878–1887, 1987. doi:10.1152/jappl.1987.62.5.1878.
39. Xu L, Yang Y, Zuo YY. Atomic force microscopy imaging of adsorbed pulmonary surfactant films. *Biophys J* 119: 756–766, 2020. doi:10.1016/j.bpj.2020.06.033.
40. Lee J, Patel DS, Stähle J, Park S-J, Kern NR, Kim S, Lee J, Cheng X, Valvano MA, Holst O, Knirel YA, Qi Y, Jo S, Klauda JB, Widmalm G, Im W. CHARMM-GUI membrane builder for complex biological membrane simulations with glycolipids and lipoglycans. *J Chem Theory Comput* 15: 775–786, 2019. doi:10.1021/acs.jctc.8b01066.
41. Irwin JJ, Shoichet BK. ZINC—a free database of commercially available compounds for virtual screening. *J Chem Inf Model* 45: 177–182, 2005. doi:10.1021/ci049714+.
42. Abraham MJ, Murtola T, Schulz R, Páll S, Smith JC, Hess B, Lindahl E. GROMACS: high performance molecular simulations through multi-level parallelism from laptops to supercomputers. *SoftwareX* 1–2: 19–25, 2015. doi:10.1016/j.softx.2015.06.001.
43. Kumar S, Rosenberg JM, Bouzida D, Swendsen RH, Kollman PA. The weighted histogram analysis method for free-energy calculations on biomolecules. I. The method. *J Comput Chem* 13: 1011–1021, 1992. doi:10.1002/jcc.540130812.
44. Hub JS, de Groot BL. Does CO<sub>2</sub> permeate through aquaporin-1? *Biophys J* 91: 842–848, 2006. doi:10.1529/biophysj.106.081406.
45. Gillman IG, Kistler KA, Stewart EW, Paolantonio AR. Effect of variable power levels on the yield of total aerosol mass and formation of aldehydes in e-cigarette aerosols. *Regul Toxicol Pharmacol* 75: 58–65, 2016. doi:10.1016/j.yrtph.2015.12.019.
46. Yang T-C, McDonald M, Morrow MR, Booth V. The effect of a C-terminal peptide of surfactant protein B (SP-B) on oriented lipid bilayers, characterized by solid-state <sup>2</sup>H- and <sup>31</sup>P-NMR. *Biophys J* 96: 3762–3771, 2009. doi:10.1016/j.bpj.2009.02.027.
47. Tashiro K, Ohta K, Cui X, Nishizuka K, Yamamoto K, Konzaki T, Kobayashi T, Suzuki Y. Effects of various forms of surfactant protein C on tidal volume in ventilated immature newborn rabbits. *J Appl Physiol* 94: 1519–1526, 2003. doi:10.1152/japplphysiol.00059.2001.
48. Greenfield NJ. Using circular dichroism spectra to estimate protein secondary structure. *Nat Protoc* 1: 2876–2890, 2006. doi:10.1038/nprot.2006.202.
49. Leigh NJ, Lawton RI, Hershberger PA, Goniewicz ML. Flavourings significantly affect inhalation toxicity of aerosol generated from electronic nicotine delivery systems (ENDS). *Tob Control* 25: ii81–ii87, 2016. doi:10.1136/tobaccocontrol-2016-053205.
50. Hsu G, Sun JY, Sh. Z. Evolution of electronic cigarette brands from 2013–2014 to 2016–2017: analysis of brand websites. *J Med Internet Res* 20: e80, 2018. doi:10.2196/jmir.8550.
51. Krüsemann EJZ, Boesveldt S, de Graaf K, Talhout R. An E-liquid flavor wheel: a shared vocabulary based on systematically reviewing e-liquid flavor classifications in literature. *Nicotine Tob Res* 21: 1310–1319, 2019.
52. Krüsemann EJZ, Havermans A, Pennings JLA, de Graaf K, Boesveldt S, Talhout R. Comprehensive overview of common e-liquid ingredients and how they can be used to predict an e-liquid's flavour category. *Tob Control* 30: 185–191, 2021. doi:10.1136/tobaccocontrol-2019-055447.
53. Hua M, Omaiye EE, Luo W, McWhirter KJ, Pankow JF, Talbot P. Identification of cytotoxic flavor chemicals in top-selling electronic cigarette refill fluids. *Sci Rep* 9: 2782–2782, 2019. doi:10.1038/s41598-019-38978-w.
54. Behar RZ, Luo W, McWhirter KJ, Pankow JF, Talbot P. Analytical and toxicological evaluation of flavor chemicals in electronic cigarette refill fluids. *Sci Rep* 8: 8288, 2018. doi:10.1038/s41598-018-25575-6.
55. Patel T, Ishiui Y, Yosipovitch G. Menthol: a refreshing look at this ancient compound. *J Am Acad Dermatol* 57: 873–878, 2007. doi:10.1016/j.jaad.2007.04.008.
56. Yang S, Wang R, Wan G, Wu Z, Guo S, Dai X, Shi X, Qiao Y. A multi-scale study on the penetration enhancement mechanism of menthol to osthole. *J Chem Inf Model* 56: 2234–2242, 2016. doi:10.1021/acs.jcim.6b00232.
57. Gusain P, Ohki S, Hoshino K, Tsujino Y, Shimokawa N, Takagi M. Chirality-dependent interaction of d- and l-menthol with biomembrane models. *Membranes (Basel)* 7: 69, 2017. doi:10.3390/membranes7040069.
58. Gaworski CL, Dozier MM, Gerhart JM, Rajendran N, Brennecke LH, Aranyi C, Heck JD. 13-Week inhalation toxicity study of menthol cigarette smoke. *Food Chem Toxicol* 35: 683–692, 1997. doi:10.1016/s0278-6915(97)00033-1.
59. Nair V, Tran M, Behar RZ, Zhai S, Cui X, Phandthong R, Wang Y, Pan S, Luo W, Pankow JF, Volz DC, Talbot P. Menthol in electronic cigarettes: a contributor to respiratory disease? *Toxicol Appl Pharmacol* 407: 115238, 2020. doi:10.1016/j.taap.2020.115238.
60. Romberg AR, Miller Lo EJ, Cuccia AF, Willett JG, Xiao H, Hair EC, Vallone DM, Marynak K, King BA. Patterns of nicotine concentrations in electronic cigarettes sold in the United States, 2013–2018. *Drug Alcohol Depend* 203: 1–7, 2019. doi:10.1016/j.drugalcdep.2019.05.029.
61. Zhang H, Wang YE, Fan Q, Zuo YY. On the low surface tension of lung surfactant. *Langmuir* 27: 8351–8358, 2011. doi:10.1021/la201482n.
62. Yang Y, Xu L, Dekkers S, Zhang LG, Cassee FR, Zuo YY. Aggregation state of metal-based nanomaterials at the pulmonary surfactant film determines biophysical inhibition. *Environ Sci Technol* 52: 8920–8929, 2018. doi:10.1021/acs.est.8b02976.
63. Hu GQ, Jiao B, Shi XH, Valle RP, Fan QH, Zuo YY. Physicochemical properties of nanoparticles regulate translocation across pulmonary surfactant monolayer and formation of lipoprotein corona. *ACS Nano* 7: 10525–10533, 2013. doi:10.1021/nn4054683.
64. Fan Q, Wang YE, Zhao X, Loo JS, Zuo YY. Adverse biophysical effects of hydroxyapatite nanoparticles on natural pulmonary surfactant. *ACS Nano* 5: 6410–6416, 2011. doi:10.1021/nn2015997.
65. Loney RW, Panzuela S, Chen J, Yang Z, Fritz JR, Dell Z, Corradi V, Kumar K, Tieleman DP, Hall SB, Tristram-Nagle SA. Location of the hydrophobic surfactant proteins, SP-B and SP-C, in fluid-phase bilayers. *J Phys Chem B* 124: 6763–6774, 2020. doi:10.1021/acs.jpcc.0c03665.
66. Chavarha M, Loney RW, Rananavare SB, Hall SB. Hydrophobic surfactant proteins strongly induce negative curvature. *Biophys J* 109: 95–105, 2015. doi:10.1016/j.bpj.2015.05.030.
67. Cabré EJ, Martínez-Calle M, Prieto M, Fedorov A, Olmeda B, Loura LMS, Pérez-Gil J. Homo- and hetero-oligomerization of hydrophobic pulmonary surfactant proteins SP-B and SP-C in surfactant phospholipid membranes. *J Biol Chem* 293: 9399–9411, 2018. doi:10.1074/jbc.RA117.000222.
68. Erythropel HC, Jabba SV, DeWinter TM, Mendizabal M, Anastas PT, Jordt SE, Zimmerman JB. Formation of flavorant–propylene glycol adducts with novel toxicological properties in chemically unstable e-cigarette liquids. *Nicotine Tob Res* 21: 1248–1258, 2019. doi:10.1093/ntr/nty192.

69. **Sleiman M, Logue JM, Montesinos VN, Russell ML, Litter MI, Gundel LA, Destailats H.** Emissions from electronic cigarettes: key parameters affecting the release of harmful chemicals. *Environ Sci Technol* 50: 9644–9651, 2016. doi:[10.1021/acs.est.6b01741](https://doi.org/10.1021/acs.est.6b01741).
70. **Czégény Z, Bozi J, Sebestyén Z, Blazsó M, Jakab E, Barta-Rajnai E, Forster M, Nicol J, McAdam KG, Liu C.** Thermal behaviour of selected flavour ingredients and additives under simulated cigarette combustion and tobacco heating conditions. *J Anal Appl Pyrol* 121: 190–204, 2016. doi:[10.1016/j.jaap.2016.07.020](https://doi.org/10.1016/j.jaap.2016.07.020).
71. **Cadham CJ, Sanchez-Romero LM, Fleischer NL, Mistry R, Hirschtick JL, Meza R, Levy DT.** The actual and anticipated effects of a menthol cigarette ban: a scoping review. *BMC Public Health* 20: 1055, 2020.
72. **Guagliardo R, Pérez-Gil J, De Smedt S, Raemdonck K.** Pulmonary surfactant and drug delivery: focusing on the role of surfactant proteins. *J Control Release* 291: 116–126, 2018. doi:[10.1016/j.jconrel.2018.10.012](https://doi.org/10.1016/j.jconrel.2018.10.012).